ISSN 0036-0236, Russian Journal of Inorganic Chemistry, 2010, Vol. 55, No. 10, pp. 1620–1629. © Pleiades Publishing, Ltd., 2010.
Original Russian Text © D.M. Babanly, M.B. Babanly, 2010, published in Zhurnal Neorganicheskoi Khimii, 2010, Vol. 55, No. 10, pp. 1715–1724.

PHYSICOCHEMICAL ANALYSIS OF INORGANIC SYSTEMS

Phase Equilibria in the Tl–TlBr–Te System and Thermodynamic Properties of the Compound Tl_5Te_2Br

D. M. Babanly and M. B. Babanly
Baku State University, 370148 Baku, Azerbaijan
e-mail: babanly_mb@rambler.ru
Received February 12, 2009

Abstract—The Tl–TlBr–Te composition region of the Tl–Te–Br phase diagram has been explored by DTA, X-ray diffraction, microhardness measurements, and electromotive force (emf) measurements relative to a thallium electrode in concentrations cells. The phase diagrams along a number of joins, the isothermal section at 400 K of the phase diagram, and a projection of the liquidus surface have been constructed. Extensive phase-separation areas, including a three-liquid-phase field in the Tl–TlBr–Tl_2Te subsystem, have been revealed. The homogeneity ranges and primary crystallization fields of phases have been mapped, and the coordinates of nonvariant and univariant equilibria in the *T–x–y* diagram have been determined. The standard thermodynamic functions of formation of the Tl_5Te_2Br compound and its standard entropy have been derived from emf data.

DOI: 10.1134/S0036023610100219

Metal chalcogenides and phases based on them are promising functional materials. Many of them possess a unique combination of semiconducting, photoelectric, thermoelectric, ferroelectric, and other properties [1, 2].

For developing the scientific foundations of the synthesis of complex phases with preset properties, it is necessary to study the phase equilibria and thermodynamic properties of the corresponding systems. Earlier, we reported integrated studies of a number of Tl–X–Hal systems (X = chalcogen, Hal = halogen) [3–8]. Here, we report the Tl–TlBr–Te system.

The Tl–Te–Br system has been explored inadequately [9, 10]. The compound Tl_2TeBr_6 was synthesized, and its homogeneity range was determined [9]. It was established by X-ray diffraction that Tl_2TeBr_6 crystallizes in the tetragonal system (space group *P*4/*nmc*) with init cell parameters of $a = 7.468$ Å and $c = 10.682$ Å ($Z = 2$) [10].

We studied the Tl–Te–Br system along a number of joins [11–15]. We synthesized Tl_5Te_2Br [11], a new thallium telluride bromide. This compound melts with decomposition via a syntectic reaction at 750 K and crystallizes in a Tl_5Te_3-type tetragonal lattice (space group *I*4/*mcm*) with unit cell parameters of $a = 8.926$ Å and $c = 12.802$ Å ($Z = 4$).

The TlBr–Te system [12] is pseudobinary, with a monotectic equilibrium at 729 ± 5 K and a degenerate eutectic equilibrium at 720 K. At the monotectic temperature, the phase separation range is 7–93 mol % Te.

The TlBr–TlTe [13], TlBr–Tl_2Te_3, and Tl_5Te_2Br–Tl(TlTe) [14] joins are not pseudobinary because of the incongruent melting of one or both of the initial compounds. The first two joins are characterized by an extensive two-liquid-phase field; the Tl_5Te_2Br–Tl join, by a three-liquid-phase field. Below the solidus, all of the alloys along these joins are two-phase mixtures of the initial phases. In the Tl_5Te_2Br–TlTe system [14], we observed a large field of Tl_5Te_2Br-based solid solutions extending extending up to ~20 mol % TlTe.

The Tl_5Te_2Br–Tl_5Te_3 system [15] is not pseudobinary either. Its specific feature is that it has both a continuous series of solid solutions and an extensive phase separation field. The primary crystallization of solid solutions in the 0–55 mol % Tl_5Te_3 range takes place via a syntectic reaction.

The binary constituent Tl–Te of the Tl–TlBr–Te system was studied by many authors. According to the *T–x* diagram based on a number of studies [16], the compounds Tl_5Te_3, TlTe, and Tl_2Te_3 form in this binary system. The first compound melts congruently at 726 K, and the last two melt incongruently at at 573 and 511 K, respectively. The Tl_5Te_3 and TlTe compounds crystallize in the tetragonal system with the following crystallographic parameters: *Cc*, $a = 8.929$ Å, $c = 12.620$ Å, $Z = 4$, space group *I*4/*mcm* [17]; TlTe, $a = 12.950$ Å, $c = 6.175$ Å, $Z = 16$ [18] (or $a = 18.229$ Å, $c = 6.157$ Å, $Z = 32$, space group $P4_2/nmc$ [19]). Tl_2Te_3 has a monoclinic structure: space group Tl_5Te_3, $a = 17.413$ Å, $b = 6.552$ Å, $c = 7.910$ Å, $\beta = 133.6°$, $Z = 4$ [17].

Along with the above compounds, the compound Tl_2Te was reported to exist in the Tl–Te system [20]. This compound melts congruently at 698 K and forms an eutectic with Tl_5Te_3 (695 K, ~34 at. % Te) [20]. These data were verified by later studies [21, 22]. Nevertheless, the existence of the Tl_2Te compound was

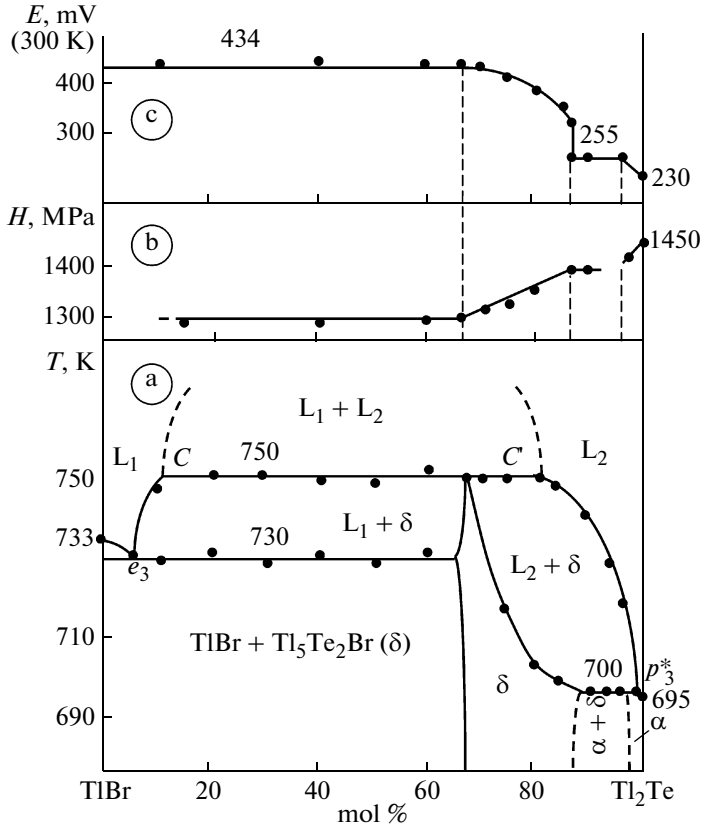

Fig. 1. (a) T–x, (b) H–x, and (c) E–x diagrams of the TlBr–Tl_2Te system.

questioned by some authors [23] until its crystal structure was determined based on 1989 reflections [24]. This compound crystallizes in the monoclinic system and has its individual structure type (space group C_2/C, a = 15.662 Å, b = 8.987 Å, c = 31.196 Å, β = 100.76°, Z = 44). The Tl_2Te lattice has both fragments characteristic of Tl_5Te_3 and fragments consisting only of thallium atoms forming Tl–Tl bonds [24].

We did not find any data on phase equilibria in the Tl–Br binary constituent. Thallium monobromide melts congruently at 733 K and has a cubic structure with a unit cell parameter of a = 3.861 Å [25].

EXPERIMENTAL

Initially, we obtained the compounds Tl_2Te, TlBr, and Tl_5Te_2Br. Tl_2Te was synthesized by the sealed-tube method from high-purity thallium and tellurium (impurity level of 10^{-3} wt % or below) in vacuo (~10^{-2} Pa). The alloying temperature was 750 K.

The synthesis of TlBr was carried out via a standard procedure [26]. Thallium metal was dissolved in dilute sulfuric acid (7–10 mol %) at ~350 K to obtain a Tl_2SO_4 solution. Next, dilute HBr was added to a boiling 2% Tl_2SO_4 solution until complete precipitation. TlBr is difficult to recrystallize. For this reason, traces of the mother liquor were removed by multiple boiling with water followed by thorough vacuum filtration. The product was dried over KOH in a desiccator at 390–400 K and was stored in the dark in order to prevent its decomposition.

The ternary compound Tl_5Te_2Br was synthesized by alloying appropriate amounts of the synthesized TlBr and Tl_2Te in a vacuumized quartz tube. This compound decomposes via a syntectic reaction upon melting [11]. For this reason, the tube containing the melt was cooled slowly to 740 K, a temperature point between the syntectic equilibrium (750 K) and the eutectic equilibrium (730 K), and was held at this temperature for ~100 h.

The synthesized compounds were identified by DTA and X-ray diffraction.

By alloying the above compounds with elementary tellurium and thallium, we prepared alloys along the Tl_2Te–[Tl_2Br], Tl_2Te–[TlTeBr], and Tl_5Te_2Br–Te joins (hereafter, heterogeneous alloys used as a "component" are enclosed in brackets) and a number of samples in the Tl–TlBr–Te region. The compositions of the latter were chosen based on the Tl–Te phase diagram [20] and earlier data on internal joins of the Tl–TlBr–Te diagram [10–15]. Taking into account the absence of phase equilibrium data for the Tl–Br system, we prepared Tl–Br alloys containing 51, 52, 55, 70, 95, 98, and 99 at. % Tl. The alloys were equili-

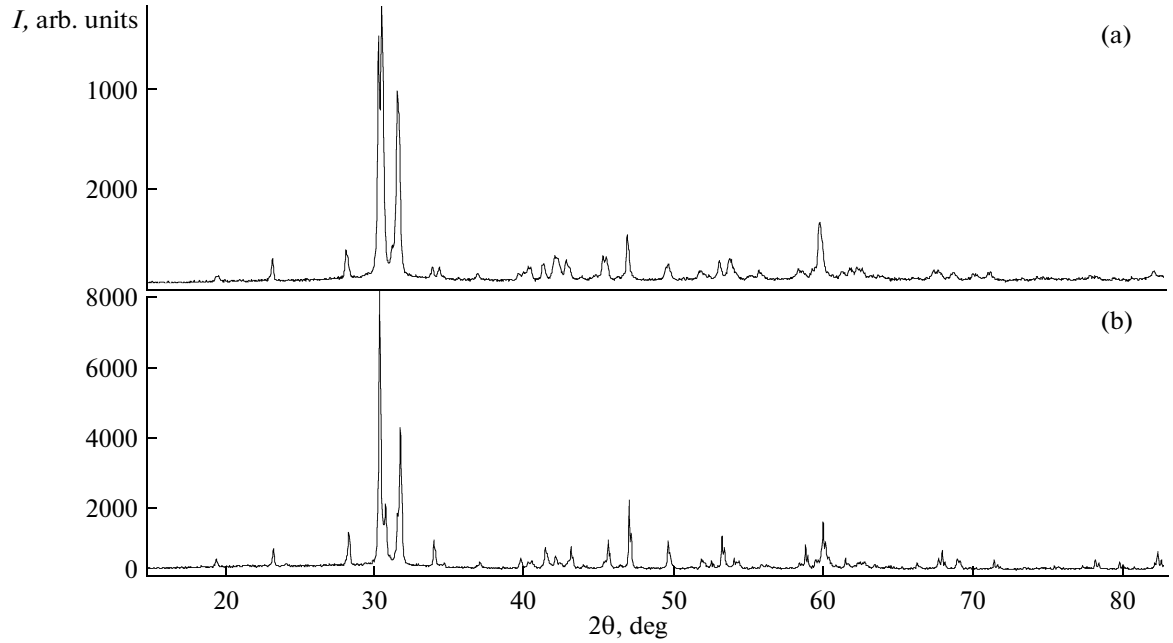

Fig. 2. X-ray diffraction patterns of (a) the compound Tl_5Te_2Br and (b) the TlBr–Tl_2Te alloy containing 85 mol % Tl_2Te.

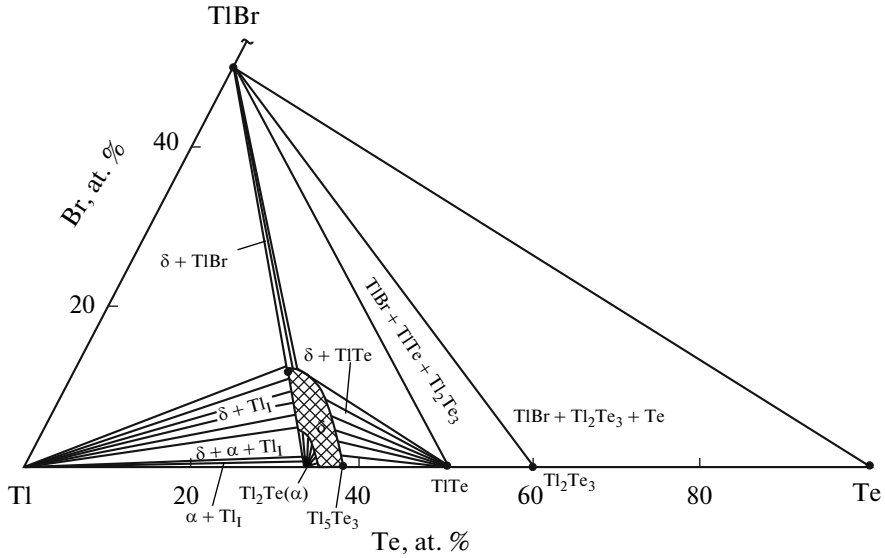

Fig. 3. Isothermal section at 300 K of the Tl–TlBr–Te phase diagram.

brated by annealing them 20–30 K below the solidus for 500–1000 h. The sample size was 0.5 g for DTA and 1 g for the other characterization methods.

Alloys were characterized by DTA (NTR-72 pyrometer, chromel–alumel thermocouples), X-ray diffraction (X'Pert MPD diffractometer, Philips, Almelo, Netherlands, Cu$K_{\alpha 1}$ radiation), microhardness measurements (PMT-3 tester, 20 g load), and electromotive force (emf) measurements in concentration cells of the type

$$(-)\mathrm{Tl\,(s)/liquid\ electrolyte} + \mathrm{Tl^+/(Tl{-}Te{-}Br)(s)(+)} \quad (1)$$

at 300–430 K. The electrolyte was a glycerol solution of KBr containing ~0.5 wt % TlBr. One of the electrodes was thallium metal, which does not react with glycerol [27]. The other electrode was a presynthesized Tl–TlBr–Te alloy from the TlBr–Tl_2Te–Te region.

Emf was measured by a compensation method using a V7-34A high-resistance digital voltmeter.

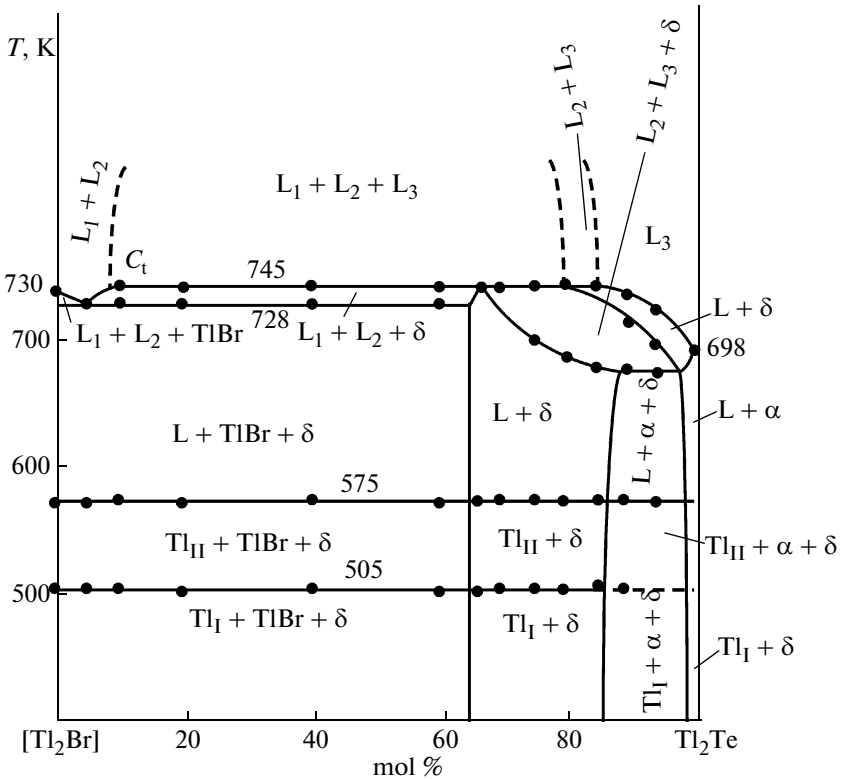

Fig. 4. $[Tl_2Br]$–Tl_2Te join of the Tl–TlBr–Te diagram.

Making electrochemical cells (1) and emf measurements are detailed elsewhere [28].

RESULTS AND DISCUSSION

For all Tl–Br alloys from the Tl–TlBr composition range, DTA data indicate well-defined temperature arrests at 505, 575, and 732 K. The first two temperatures are equal to the polymorphic transition and melting temperatures of thallium, and the third coincides with the melting point of pure TlBr within ±1 K. Therefore, the components of the Tl–TlBr subsystem are separated throughout its composition range.

Processing experimental data for the Tl–TlBr–Te system, we took into consideration the T–x diagrams of the other boundary systems—Tl–Te [20] and TlBr–Te [12]—and those of internal joins [11, 13–15].

Our study provided full information concerning phase equilibria in the Tl–TlBr–Te system (Figs. 1–6). The types and coordinates of all nonvariant and univariant equilibria, including those for the constituent binary systems, are listed in Tables 1 and 2.

Alloys of the TlBr–Tl_2Te join, particularly those containing over 60 mol % Tl_2Te, are difficult to homogenize [11]. For this reason, in order to obtain samples equilibrated to the maximum possible extent, cast alloys from this composition region were ground into a powder and pressed into pellets prior to being annealed at 720 K. This operation was repeated every 300 h during annealing. The total annealing time was ~900 h.

Examination of the samples annealed in this way suggested some changes to the T–x diagram of the TlBr–Tl_2Te system (Fig. 1a). According to the refined phase diagram, the homogeneity range of the Tl_5Te_2Br-based δ-phase is not 66.6–80 mol % Tl_2Te [11], but 66.6–87 mol % Tl_2Te, and the solidus temperature is higher by 15–20 K (Fig. 1a).

X-ray diffraction, emf, and microhardness data confirm the results of DTA.

The X-ray diffraction patterns of TlBr–Tl_2Te alloys from the homogeneity range of the δ-phase almost coincide with that of Tl_5Te_2Br and show no reflections characteristic of Tl_2Te (Fig. 2).

The microhardness of Tl_5Te_2Br is 1300 MPa throughout the TlBr–Tl_5Te_2Br phase field and increases monotonically to ~1400 MPa in the composition range from 66.7 to 87 mol % Tl_2Te. The microhardness of the Tl_2Te phase decreases slightly from 1450 to 1420 MPa with an increasing percentage of TlBr (Fig. 1b).

The emf isotherm at 300 K (Fig. 1c) has two plateaus at 434 and 255 mV, which correspond to the TlBr + δ and δ + α two-phase fields. In the composition range from 66.7 to 85 mol % Tl_2Te, which is the homogeneity range of the δ-phase, E decreases monotonically

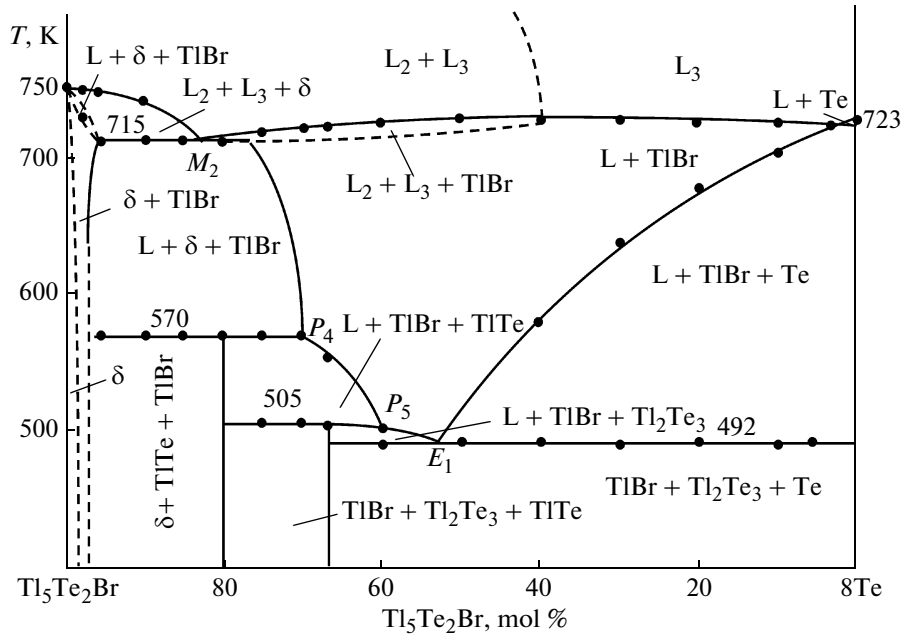

Fig. 5. Tl_5Te_2Br–Te join of the Tl–TlBr–Te diagram.

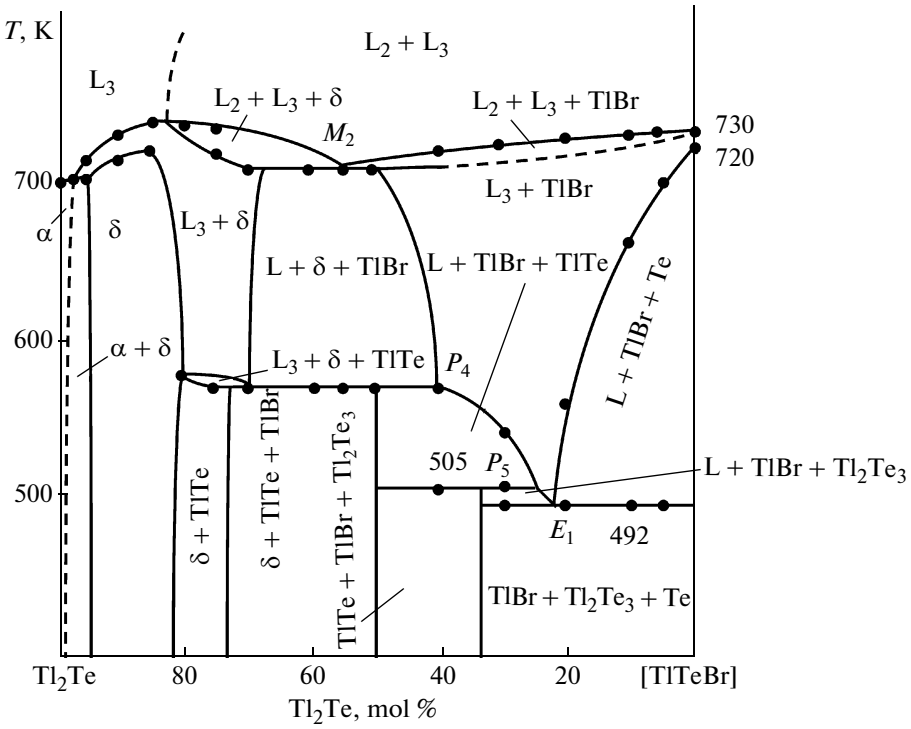

Fig. 6. Tl_2Te–[TlTeBr] join of the Tl–TlBr–Te diagram.

from 434 to 330 mV. The emf value in the α + δ field (~255 mV) is well above the emf measured for pure Tl_2Te (~230 mV [29]), indicating the existence of some homogeneity range of Tl_2Te (~2–3 mol %, α-phase).

The 300-K isothermal section of the Tl–TlBr–Te diagram (Fig. 3) illustrates the subsolidus phase relations, including the wide homogeneity range of Tl_5Te_2Br (δ-phase). The homogeneity range of the

Table 1. Nonvariant equilibria in the Tl–TlBr–Te system

Point in Fig. 7	Equilibrium	Composition, at. %			T, K
		Tl	Te	Br	
D_1	$L_{D_1} \rightleftharpoons Tl_2Te(\alpha)$	66.7	33.3	–	698
D_2	$L_{D_2} \rightleftharpoons Tl_5Te_3(\delta)$	62.5	37.5	–	723
D_3	$L_{D_3} \rightleftharpoons TlBr$	50	–	50	733
e_1	$L \rightleftharpoons \alpha + \delta$	66	34	–	695
e_2	$L \rightleftharpoons Tl_2Te_3 + Te$	30	70	–	497
e_3	$L \rightleftharpoons TlBr + \delta$	51.5	~2	46.5	730
e_4^*	$L \rightleftharpoons TlBr + Te$	~0.5	~99	~0.5	720
e_5^*	$L \rightleftharpoons Tl_{II} + TlBr$	~100	–	–	573
e_6^*	$L \rightleftharpoons Tl_{II} + \alpha$	~100	–	–	573
E_1	$L \rightleftharpoons TlBr + Tl_2Te_3 + Te$	30	69	~1	492
E_2^*	$L \rightleftharpoons Tl_{II} + \alpha + \delta$	~100			~573
P_1	$L + \delta \rightleftharpoons TlTe$	43	57	–	573
P_2	$L + TlTe \rightleftharpoons Tl_2Te_3$	35	65	–	508
P_3^*	$L + \delta \rightleftharpoons \alpha$	~67	~32	~1	700
P_4	$L + \delta \rightleftharpoons TlBr + TlTe$	42	56.5	1.5	570
P_5	$L + TlTe \rightleftharpoons TlBr + Tl_2Te_3$	34.5	64.5	~1	505
P_6^*	$L + TlBr \rightleftharpoons Tl_{II} + \delta$	~100			573
$m_1(m_1')$	$L_3 \rightleftharpoons L_1 + \delta(\alpha^*)$	69.5(95)	30.5(5)	–	681
$m_2(m_2^*)$	$L_2 \rightleftharpoons L_1 + TlBr$	51(99)	–	49(~1)	732
$m_3(m_3^*)$	$L_2 \rightleftharpoons L_3 + TlBr$	47(4)	6(92)	47(4)	730
$C(C')$	$L_2 + L_3 \rightleftharpoons Tl_5Te_2Br(d)$	52.5(65)	5(28)	42.5(7)	750
$M_1(M_1^*)$	$L_2 \rightleftharpoons L_1 + TlBr + \delta$	52.5(~100)	1.5	46	728
$M_2(M_2')$	$L_2 \rightleftharpoons L_3 + TlBr + \delta$	50(52)	6(43)	44(5)	715
M_3^*	$L_3 + d \rightleftharpoons L_1 + \alpha$	~69	30.5	~0.5	682
$C_t(C_t'; C_t^*)$	$L_2 + L_3 \rightleftharpoons L_1 + \delta$	54(68; ~100)	4(27)	42(5)	745

Table 2. Univariant equilibria in the Tl–TlBr–Te system

Curve in Fig. 7	Equilibrium	Temperature range, K
e_2E_1	$L \rightleftharpoons Tl_2Te_3 + Te$	497–492
e_3M_1	$L \rightleftharpoons TlBr + \delta$	730–728
e_3M_2	$L \rightleftharpoons TlBr + \delta$	730–715
M'_2P_4	$L \rightleftharpoons TlBr + \delta$	715–568
P_1P_4	$L + \delta \rightleftharpoons TlTe$	573–570
P_4P_5	$L \rightleftharpoons \delta + TlTe$	568–505
P_2P_5	$L + TlTe \rightleftharpoons Tl_2Te_3$	508–505
P_5E_1	$L \rightleftharpoons Tl_2Te_3 + Te$	505–492
$e_4^*E_1$	$L \rightleftharpoons TlBr + Te$	720–492
$m_2M_1(m_2^*M_1^*)$	$L_2 \rightleftharpoons L_1 + TlBr$	732–728
$C_tM_1(C_t^*M_1^*)$	$L_1 + L_2 \rightleftharpoons \delta$	745–728
$C'_tM_3(C_t^*M'^*_3)$	$L_1 + L_3 \rightleftharpoons \delta$	745–682
$m_3M_2(m'_3M'_2)$	$L_2 \rightleftharpoons L_3 + TlBr$	730–715
$CC_t(C'C'_t)$	$L_2 + L_3 \rightleftharpoons \delta$	750–745
$CM_2(C'M'_2)$	$L_2 + L_3 \rightleftharpoons \delta$	750–715

δ-phase extends far beyond the TlBr–Tl_2Te join toward excess tellurium, appearing as a broad continuous band representing the Tl_5Te_3-based berthollide (34.5–38 at % Te [20]) in the Tl–Te diagram.

The dominant role in the subsolidus phase relations (Fig. 3) is played by TlBr, the thermodynamically most stable compound in the Tl–Te–Br system. This compound forms stable tie lines with all the other phases but Tl_5Te_3 and is a constituent of the three-phase fields Tl + δ + TlBr, TlBr + TlTe + δ, TlBr + TlTe + Tl_2Te_3, and TlBr + Tl_2Te_3 + Te. The compound Tl_5Te_2Br and the δ-phase based on this compound are in two-phase equilibria with TlBr, TlTe, and Tl.

It is convenient to examine phase equilibria along complicated joins (Figs. 4–6) simultaneously with the projection of the *T–x–y* diagram (Fig. 7).

The [Tl_2Br]–Tl_2Te join (Fig. 4) is characterized by an extensive three-liquid-phase field ($L_1 + L_2 + L_3$, ~10–70 mol % Tl_2Te), which borders the two-liquid-phase fields $L_1 + L_2$ and $L_2 + L_3$ (L_1, L_2, and L_3 are liquid solutions based on thallium metal, TlBr, and tellurides, respectively). The DTA profiles for the alloys from this join indicate up to four or even five thermal events. The horizontal lines at 505 and 575 K in Fig. 4 are due to the polymorphic transition and melting of thallium. The lines at 728 and 745 K represent a four-phase monotectic equilibrium (M_1) and a four-phase syntectic equilibrium (C_t), respectively (Figs. 4, 7, Table 1). Below the solidus line, this join crosses the following four phase fields: $Tl_1 + \alpha$, $Tl_1 + \alpha + \delta$, $Tl_1 + \delta$, and Tl_1 + TlBr + δ.

The Tl_5Te_2Br–Te join (Fig. 5) illustrates the phase equilibria in the TlBr–Tl_2Te–Te composition region. Below the solidus, it crosses the following five phase fields δ, δ + TlBr, δ + TlBr + TlTe, TlBr + Tl_2Te_3 + Te, and Tl_2Te_3 + TlBr + Te. This is in full agreement with the subsolidus phase diagram presented in Fig. 3. The data obtained for this join prompted us to refine primary crystallization and phase separation fields, univariant equilibrium curves, and the coordinates of some nonvariant points in the Tl–TlBr–Te diagram (Fig. 7, Tables 1, 2).

The liquidus line along the Tl_5Te_2Br–Te join consists of the two curves corresponding to the primary crystallization of TlBr and the δ-phase. Two liquid phases ($L_1 + L_2$) coexist in the composition range from 40 to 100 mol % Tl_5Te_2Br. The primary crystallization of the δ-phase from this two-phase melt takes place between 82 and 100 mol % Tl_5Te_2Br; the primary crystallization of TlBr, in the composition range of ~40–82 mol % Tl_5Te_2Br. The total width of the TlBr primary crystallization field is ~3–82 mol % Tl_5Te_2Br (Fig. 5).

Tl_2Te–[TlTeBr] join (Fig. 6). The phase equilibria along this join are qualitatively similar to those for the Tl_5Te_2Br–Te join. This is due to the fact these joins cross the same phase fields of the *T–x–y* diagram. The liquidus consists of the TlBr and δ-phase primary crystallization curves (Fig. 6). Well-defined univariant equilibrium curves (M_2P_4, P_4P_5, P_5E_1) and nonvariant equilibrium points (M_2, P_4, P_5, E_1) can be seen in the phase diagram for this join (Tables 1, 2).

The liquidus surface for the Tl–TlBr–Te system (Fig. 7) consists of the five fields corresponding to the primary crystallization of TlBr, δ-phase, TlTe, Tl_2Te_3, and Te. The liquidus surfaces of Tl_2Te (α) and elementary thallium are degenerate.

A specific feature of the Tl–TlBr–Te system is that it has extensive liquid phase separation fields made up by the following phases: liquid based on thallium (L_1); liquid based on TlBr (L_2); and liquid consisting of the δ-phase, tellurides, and elementary tellurium (L_3). These fields occupy over 90% of the Tl–TlBr–Te concentration triangle. The system has an extensive three-liquid-phase field, $C_tC'_tC_t^*$ (Fig. 7), which is sur-

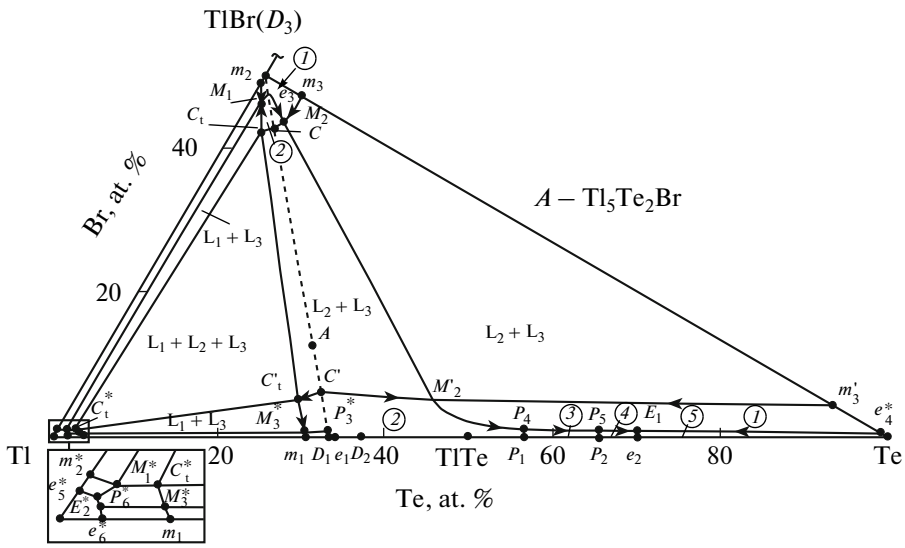

Fig. 7. Projection of the liquidus surface of the Tl–TlBr–Te diagram. Primary crystallization fields: (*1*) TlBr, (*2*) δ-phase based on Tl_5Te_2Br, (*3*) TlTe, (*4*) Tl_2Te_3, and (*5*) Te. The dashed line shows the TlBr–Tl_2Te pseudobinary join.

rounded by two-liquid-phase fields. The $C_tC'_tC^*_t$ triangle is indicates the nonvariant syntectic equilibrium $L_1 + L_2 + L_3 \rightleftharpoons \delta$ (Table 1). The formation of the three-liquid-phase field is due to the presence of extensive liquid/liquid phase separation fields on the sides of the concentration triangle of the Tl–TlBr–Tl_2Te subsystem ($m_1m'_1$, $m_2m^*_2$, CC'). Hereafter, stars label degenerate points.

The liquid/liquid phase separation fields CC' and $m_3m'_3$ in the TlBr–Tl_2Te and TlBr–Te pseudobinary systems jut out into the TlBr–Tl_2Te–Te subsystem to form a broad continuous phase separation band, $L_2 + L_3$. The eutectic curve, which originates from the point e_3, crosses this phase separation field. The horizontal line $M_2M'_2$, which represents a nonvariant monotectic equilibrium, appears as a result (Table 1).

Phase crystallization in the phase separation fields occurs via nonvariant and univariant monotectic and syntectic reactions (Fig. 7, Tables 1, 2).

The types of nonvariant equilibria and the coordinates of the corresponding points are presented in Table 1. The temperature ranges of the univariant equilibria are listed in Table 2.

The results of emf measurements in cell (1) for TlBr–Tl_2Te–Te samples, which are fully consistent with the subsolidus phase relations (Fig. 3), enabled us to calculate thermodynamic functions of the ternary compound Tl_5Te_2Br. Since the temperature dependence of emf was linear, the emf data were fitted by least squares [30] to the equation $E = a + bT \pm tS_E(T)$ [31] (Table 3). We found that, within each of the three-phase fields TlBr–TlTe–δ, TlBr–TlTe–Tl_2Te_3, and TlBr–Tl_2Te_3–Te, emf is independent of the alloy composition. In the last two fields, the emf value is equal, within ±3 mV, to that reported for pure TlTe and Tl_2Te_3, respectively [29]. Firstly, this is evidence of the

Table 3. Emf as a function of temperature over the 300–430 K range for cell (1)

Phase field in Fig. 3	$E\,(\text{mV}) = a + bT \pm 2\left[S_E^2/n + S_E^2\left(T_i - \overline{T}\right)^2 \Big/ \sum(T_i - \overline{T})^2\right]^{1/2}$
Tl_5Te_2Br + TlBr + TlTe	$435.5 + 0.003T \pm 2\left[1.70/22 + 5.3\times10^{-5}(T - 360.4)^2\right]^{1/2}$
TlBr + TlTe + Tl_2Te_3	$428.5 + 0.032T \pm 2\left[1.72/22 + 4.7\times10^{-5}(T - 361.8)^2\right]^{1/2}$
TlBr + Tl_2Te_3 + Te	$446.5 + 0.048T \pm 2\left[0.92/22 + 2.8\times10^{-5}(T - 361.8)^2\right]^{1/2}$

Table 4. Standard integrated thermodynamic function of the compounds Tl_5Te_2Br, TlBr, and TlTe

Compound	$-\Delta G^0_{298}$	$-\Delta H^0_{298}$	S^0_{298}
	kJ/mol		J/(mol K)
TlBr [32]	167.4 ± 0.6	172.7 ± 0.7	122.6 ± 0.2
TlTe [29]	44.5 ± 0.4	43.9 ± 0.5	115.9 ± 1.6
Tl_5Te_2Br	340.6 ± 1.6	344.5 ± 2.7	483.4 ± 6.2

reversibility of cell (1). Secondly, this corroborates our data indicating small extents of solid solution in TlTe and Tl_2Te_3 in the Tl–TlBr–Te system.

Using familiar thermodynamic relationships and the equations for emf as a function of temperature for the TlBr–Tl_5Te_2Br–TlTe three-phase field (Table 3), we calculated the following relative molar functions of thallium at 298 K:

$$\overline{\Delta G}_{\mathrm{Tl}} = -(42.11 \pm 0.10)\ \ \mathrm{kJ/mol};$$

$$\overline{\Delta H}_{\mathrm{Tl}} = -(42.02 \pm 0.51)\ \mathrm{kJ/mol};$$

$$\overline{\Delta S}_{\mathrm{Tl}} = 0.29 \pm 1.40\ \ \ \mathrm{kJ/(mol\ K)}.$$

According to the solid-phase equilibrium diagram (Fig. 3), these functions are thermodynamic characteristics of the following potential-forming reaction [28]:

$$\mathrm{Tl\ (s) + 0.5TlBr\ (s) + TlTe\ (s) = 0.5Tl_5Te_2Br\ (s)}.$$

Based on this equation, the standard thermodynamic functions of formation of Tl_5Te_2Br were calculated as

$$\Delta Z^0(\mathrm{Tl_5Te_2Br}) = 2\overline{\Delta Z}_{\mathrm{Tl}} + 2\Delta Z^0(\mathrm{TlTe}) + \Delta Z^0(\mathrm{TlBr}),$$

where ΔZ–ΔG, or ΔH, and the standard entropy was calculated via the equation

$$S^0(\mathrm{Tl_5Te_2Br}) = 2\overline{\Delta S}_{\mathrm{Tl}} + 2S^0(\mathrm{Tl}) + S^0(\mathrm{TlBr}) + 2S^0(\mathrm{TlTe}).$$

In these calculations we used our own $\overline{\Delta Z}_{\mathrm{Tl}}$ data, the standard thermodynamic functions of formation of TlBr [32] and TlTe [29] (Table 4), and the standard entropy of thallium [32].

The results of these calculations are presented in Table 4. Errors were determined by the error accumulation method.

REFERENCES

1. E. I. Gerzanich and V. M. Fridkin, *$A^VB^{VI}C^{VIII}$ Ferroelectrics* (Nauka, Moscow, 1982) [in Russian].
2. M. G. Konatzidis, *Semiconductors and Semimetals*, Ed. by T. M. Tritt (Academic Press, San Diego/San Francisco/ NwYork/Boston/London/Sydney/Tokio, 2001).
3. M. B. Babanly, G. M. Guseinov, D. M. Babanly, and F. M. Sadygov, Zh. Neorg. Khim. **51** (5), 876 (2006) [Russ. J. Inorg. Chem. **51** (5), 810 (2006)].
4. D. M. Babanly, Yu. A. Yusibov, and M. B. Babanly, Zh. Neorg. Khim. **52** (5), 819 (2007) [Russ. J. Inorg. Chem. **52** (5), 753 (2007)].
5. D. M. Babanly, Yu. A. Yusibov, and M. B. Babanly, Zh. Neorg. Khim. **52** (5), 827 (2007) [Russ. J. Inorg. Chem. **52** (5), 761 (2007)].
6. R. A. Alieva, I. M. Babanly, D. M. Babanly, and I. I. Aliev, Vestn. Baku Gos. Univ., Ser. Estestv. Nauk, No. 4, 83, (2004).
7. R. A. Alieva, I. M. Babanly, D. M. Babanly, and I. I. Aliev, Khim. Problemy No. 4, 83 (2004).
8. M. B. Babanly, G. M. Guseinov, D. M. Babanly, and F. M. Sadygov, Khim. Problemy No. 2, 141 (2007).
9. E. Yu. Peresh, O. V. Zubaka, S. V. Kun, et al., Neorg. Mater. **37** (8), 1000 (2001).
10. V. I. Sidey, O. V. Zubaka, A. M. Solomon, et al., J. Alloy. Compd **367**, 115 (2004).
11. D. M. Babanly, A. A. Nadzhafova, M. I. Chiragov, and M. B. Babanly, Khim. Problemy No. 2, p. 149 (2005).
12. D. M. Babanly, I. M. Babanly, N. A. Rzaeva, and I. I. Aliev, *Proceedings of IX Republican Scientific Conference "Physicochemical Analysis and Inorganic Materials Science"* (Baku, 2004), p. 49 [in Russian].
13. D. M. Babanly, G. M. Guseinov, Yu. A. Yusibov, and F. M. Sadygov, *Proceedings of IX Republican Scientific Conference "Physicochemical Analysis and Inorganic Materials Science"* (Baku, 2004), p. 108 [in Russian].
14. D. M. Babanly and Yu. A. Yusibov, Khim. Problemy No. 2, p. 392 (2007).
15. D. M. Babanly, I. I. Aliev, Yu. A. Yusibov, and M. I. Chiragov, Azerb. Khim. Zh., No. 1, 151 (2007).
16. N. Kh. Abrikoso, V. F. Bankina, and L. V. Poretskaya, *Semiconducting Chalcogenides and Their Alloys* (Nauka, Moscow, 1975) [in Russian].
17. S. Bhan and K. Shubert, J. Less-Common Met. **20** (3), 229 (1970).
18. A. Rabenau, A. Stegherr, and P. Eckerlin, Z. Metallkd. **51** (5), 295 (1960).
19. K. Stöwe, J. Solid State Chem. **149** (1), 123 (2000).
20. M. M. Asadov, M. B. Babanly, and A. A. Kuliev, Izv. Akad. Nauk SSSR, Neorg. Mater. **13** (8), 1407 (1977).
21. H. Said and R. Castaned, Z. Metallkd. **69** (3), 281 (1978).
22. M. C. Record, Y. Feutelais, and H. L. Lukas, Z. Metallkd. **88**, 45 (1997).
23. H. Okomoto, J. Phase Equilibr. **15** (1), 131 (1994).
24. R. Cerny, J. Joubert, Y. Filinchuk, and Y. Feutelais, Acta Crystallogr., Sect. C: Cryst. Struct. Commun. **58** (5), 163 (2002).
25. H. Remy, *Lehrbuch der anorganischen Chemie* (Akademische Verlagsgesellschaft Geest und Portig, Leipzig, 1961; Mir, Moscow, 1972), Vol. 2.

26. *Handbuch der práparativen anorganischen Chemie,* Ed. by G. Brauer (Ferdinand Enke, Stuttgart, 1978; Mir, Moscow, 1985).

27. N. Ya. Turova and A. L. Novoselova, Usp. Khim. **34** (3), 385 (1956).

28. M. B. Babanly, Yu. A. Yusibov, and V. T. Abishev, *EMF Measurements in the Thermodynamics of Compound Semiconductors* (BGU, Baku, 1992) [in Russian].

29. V. P. Vasil'ev, A. V. Nikol'skaya, Ya. I. Gerasimov, and A. F. Kuznetsov, Izv. Akad. Nauk SSSR, Neorg. Mater. **4** (7), 1040 (1968).

30. K. Derffel', *Statistika v analiticheskoi khimii. Per. s nem* (Mir, Moscow, 1994) [in Russian].

31. A. N. Kornilov, L. B. Stepina, and V. A. Sokolov, Zh. Fiz. Khim. **46** (11), 2974 (1972).

32. O. Kubaschewski, C.B. Alcock, P. Spenser, *Materials Thermochemistry*. (Pergamon Press), 1993. 350 p.